PAPER

Effect of molecular crowders on ligand binding kinetics with G-quadruplex DNA probed by fluorescence correlation spectroscopy

Methods and Applications in Fluorescence

PAPER

Effect of molecular crowders on ligand binding kinetics with G-quadruplex DNA probed by fluorescence correlation spectroscopy

RECEIVED
7 May 2024

REVISED
25 June 2024

ACCEPTED FOR PUBLICATION
16 July 2024

PUBLISHED
26 July 2024

Parvez Alam[1], **Ndege Simisi Clovis**[1], **Ajay Kumar Chand**[1], **Mohammad Firoz Khan** and **Sobhan Sen**

Spectroscopy Laboratory, School of Physical Sciences, Jawaharlal Nehru University, New Delhi 110067, India

[1] Authors contributed equally.

E-mail: sens@mail.jnu.ac.in

Keywords: G-quadruplex DNA, ligand interaction kinetics, saccharide molecular crowder, fluorescence correlation spectroscopy

Supplementary material for this article is available online

Abstract

Guanine-rich single-stranded DNA folds into G-quadruplex DNA (GqDNA) structures, which play crucial roles in various biological processes. These structures are also promising targets for ligands, potentially inducing antitumor effects. While thermodynamic parameters of ligand/DNA interactions are well-studied, the kinetics of ligand interaction with GqDNA, particularly in cell-like crowded environments, remain less explored. In this study, we investigate the impact of molecular crowding agents (glucose, sucrose, and ficoll 70) at physiologically relevant concentrations (20% w/v) on the association and dissociation rates of the benzophenoxazine-core based ligand, cresyl violet (CV), with human telomeric antiparallel-GqDNA. We utilized fluorescence correlation spectroscopy (FCS) along with other techniques. Our findings reveal that crowding agents decrease the binding affinity of CV to GqDNA, with the most significant effect—a nearly three-fold decrease—observed with ficoll 70. FCS measurements indicate that this decrease is primarily due to a viscosity-induced slowdown of ligand association in the crowded environment. Interestingly, dissociation rates remain largely unaffected by smaller crowders, with only small effect observed in presence of ficoll 70 due to direct but weak interaction between the ligand and ficoll. These results along with previously reported data provide valuable insights into ligand/GqDNA interactions in cellular contexts, suggesting a conserved mechanism of saccharide crowder influence, regardless of variations in GqDNA structure and ligand binding mode. This underscores the importance of considering crowding effects in the design and development of GqDNA-targeted drugs for potential cancer treatment.

1. Introduction

Complementing the predominant Watson-Crick double stranded helix, DNA adopts diverse secondary structures including G-quadruplex DNA (GqDNA) which is formed by repetitive sequences of $d(TTAGGG)_n$ in the presence of cations. These structures are particularly prevalent in both promoter and telomeric regions [1–3]. GqDNA forms characteristic basket-like higher-order nucleic acid structures composed of two or more planar G-tetrads which are stabilized by Hoogsteen hydrogen bonding among the guanine bases in presence of cations. Interestingly, GqDNA demonstrates substantial topological polymorphism, including the conformations based on intra- and intermolecular configurations of G-tetrads as well as the cationic environment [4–9]. These structural features provide GqDNA with critical roles in various cellular processes such as modulation of chromatin structures [10, 11], protection of chromosome ends [12, 13], regulating recruitment of proteins [14, 15], transcription [16–18], DNA/RNA loop formations [19, 20], stimulation of liquid-liquid phase separation [21, 22], evocation of DNA damage-repair processes [23, 24], gene expression [25, 26], telomere shortening [27, 28], and translation [29–31]. A particularly fascinating feature of GqDNA structures also lies in their natural tendency to generate specific ligand binding sites. This unique characteristic of GqDNA has emerged as a crucial point of intense research investigations because of its promising implications in the cancer treatment. Researchers synthesized various small molecules that selectively target and stabilize GqDNA structures, but

not the duplex-DNA. This strategy led to development of several small-molecule ligands that are specific to quadruplexes and are often shown to have anticancer properties [32–38].

Previous investigations have primarily focused on elucidating the thermodynamics of ligand/biomolecule interactions [39–43]. However, there remains a paucity of data regarding the *kinetics* of such interactions, especially for the ligand/GqDNA interactions. Such kinetic information of ligand/GqDNA interaction can provide valuable insights into the association and dissociation rates which govern these interactions, particularly in more realistic cell-like crowded environments [44]. Earlier reports have emphasized the significance of ligand association and dissociation rates in determining the overall ligand binding affinity to GqDNA, albeit mostly within dilute solutions [45–47]. However, these findings have not been extensively translated to more physiologically relevant contexts such as crowded cellular environment. Our previous investigation represents the initial step which tried to address this knowledge gap by examining the impact of molecular crowding on the kinetic rates of a ligand's interaction with (3+1) hybrid type GqDNA structure [44]. We quantitatively elucidated the effects of monomer and polymers of saccharide crowders on a ligand's forward and reverse reaction rates with hybrid GqDNA, providing valuable insights into the behavior of crowder-controls of ligand interaction with GqDNA [44]. This current study delve into the influence of these saccharide crowders on the kinetics of ligand/GqDNA interaction, when the GqDNA conformation changes from hybrid to antiparallel and the ligand binding changes from a π-stacking mode to groove-binding. Such information is unknown that how these crowders may influence the kinetics of ligand binding to a groove formed by an antiparallel-GqDNA structure.

Actual cellular environment of all living organisms represents a highly complex and crowded milieu which is densely populated with a diverse array of biomolecules, encompassing nucleic acids, proteins, lipids, and small molecular crowding agents. The content of such crowders inside the cytosolic regions of various cells are different. The concentration can go up to very high values, such as the concentrations in Eukaryotic cell range in ∼50–400 mg ml^{-1}, ∼300–400 mg/ml in *E.coli*, nearly 80 mg ml^{-1} of solutes found in blood plasma, ∼270–560 mg ml^{-1} in mitochondria, and approximately 400 mg/ml of small and macromolecules inside the nucleus [48–50]. Therefore, navigating the intricate and densely populated cell-like environments to examine the structural, thermodynamic, and kinetic aspects of ligand/biomolecule interactions present a significant challenge. To circumvent such difficulties inherent in the more realistic cellular environment, current research approaches have adopted a strategy of introducing predetermined amount of background co-solutes or co-solvents into the solution, commonly referred to as molecular crowders. This allows for closer mimics of the cellular milieu under *in vitro* experimental conditions [51–64], which facilitates a more accurate representation to study ligand/biomolecule interactions, as compared to studies in traditional dilute solution [44, 63].

The molecular behaviour of various biomolecules under crowded conditions differs significantly from that observed in dilute conditions, primarily due to pronounced disturbances arising from changes in viscosity, excluded volume effects, water activity, osmotic stress, environmental polarity, and a variety of specific or non-specific interactions occurring within the crowded cellular environment. Such changes can have potential influence on the structure, dynamics, and biomolecular interactions [51–64]. Previous studies have indicated that nucleic acids, proteins, lipids, and several enzymes exhibit stabilization in the presence of certain molecular crowders, although some crowders can exert destabilizing effects [44, 53, 58, 59, 65–67]. Speer and co-workers reported the dominance of chemical reactions on the repulsions of crowders with the protein complexes which affect the stability of proteins [68, 69]. One of the studies by Gai and co-workers have investigated the role of crowding on the thermal stability and folding/unfolding kinetics of small peptides using dextran 70 and ficoll 70 as crowders where they found a negligible effect on the folding kinetics, but observed a viscosity induced decrement in the helix-to-coil transition of the peptides [70]. Patra *et al* unveiled the dynamics and kinetic rates of GqDNA/RGG peptide interaction by combining dual-colour fluorescence cross correlation spectroscopy (FCCS) and Förster resonance energy transfer (FRET) measurements [67]. Weiss and co-workers have demonstrated the size dependent enhancement in the late initiation and promoter clearance rates of RNA polymerase in the crowding conditions by using quenching-based single molecule methods and found a notable deviation from the assumptions made by scaled-particle theory [71]. There are several other studies available that focused on the G-quadruplexes and small cosolutes/ligands interaction to form stable complexes at relevant positions inside the cells that can inhibit the cancer activities [36, 37, 72]. Kovermann and co-workers studied the modulated effects of different sized crowders like EG, PEG, glucose and dextran on the binding strength of single-stranded DNA to the cold shock protein B (CspB) and showed a crowder independent retardation of association as well as an intractable dependence of dissociation on the size and chemical properties of the crowders [60]. These studies have considered both effects originating from the volume exclusion as well as soft interactions of the crowders in their *in vitro* experimental conditions. One of the *in silico* study by Dey *et al* explored the excluded volume effect on the target search dynamics of proteins on DNA in a physiological crowding condition and observed the

competing behaviour of the depletion layer and the degree of protein-crowder crosstalk. Even if the crowders enhance the overall macro-viscosity of solution, the depletion layer smoothens the DNA target search of proteins [61]. Singh and co-workers have shown the folding as well as stabilization of GqDNA structure upon binding with hydroxychloroquine (HCQ), an anti-malarial drug, in cancerous microenvironments [73, 74]. Schuler and co-workers have depicted the interaction kinetics of two intrinsically disordered proteins (IDPs) in the presence of PEGs of different molecular weights by using single molecule FRET (smFRET) technique and shown a depletion-induced acceleration along with viscosity-induced deceleration of association rates at low and high crowder concentrations, respectively [62].

Our group have previously investigated, how a ligand, cresyl violet (CV), containing benzophenoxazine group, interacts with hybrid and antiparallel-GqDNA structures in dilute aqueous buffer [45]. Our findings revealed that CV binds to (3+1) hybrid GqDNA mainly through π-π stacking interactions, while it employs a groove binding mechanism with antiparallel-GqDNA. Notably, the binding affinity of CV was stronger for (3+1) hybrid GqDNA as compared to that with antiparallel-GqDNA [45]. It is well-established that crowded environment can drastically affect the ligand binding affinity with DNA [44, 63, 75]. In a more recent study, we delved into how widely used saccharide crowders (glucose, sucrose and ficoll 70) influence the binding affinity of CV with (3+1) hybrid GqDNA [44]. Our observations indicated that the presence of 20% (w/v) mono- and polysaccharide crowders led to a decrease in association rates of the CV, π-stacked to hybrid GqDNA, primarily due to the increased local viscosity of the solution [44]. It is to be noted here that the 20% (w/v) concentration used is not only comparable to the concentrations of crowders found in cell-environment, but also these three saccharide crowders produce similar volume exclusion in solution [76, 77]. Hence, the *overall* steric effects provided by all three crowders can be considered as similar at a given concentration, such that one can exclusively observe the effects of other parameters like viscosity, dielectric environment and soft interactions on the thermodynamics and kinetics of ligand/biomolecule interactions. The choice of these crowders were also based on the fact that ficoll 70 and Xenopus laevis egg extract show similar crowding effects and also that they are rather inert crowders whose effects are minimal on the GqDNA structural change [60, 78].

Building on this knowledge, the current study aims to explore how these saccharide crowders affect the interaction kinetics between the CV and GqDNA especially when the GqDNA conformation changes from (3+1) hybrid to antiparallel structure and the binding mode of ligand changes from π-π stacking to a groove binding. For this, we have employed dual-channel fluorescence correlation spectroscopy (FCS), a high-resolution technique which is capable of measuring correlation of fluorescence fluctuations from nanoseconds to seconds, operating at the (near) single-molecule level, aided by other methods.

The interactions of small-molecular-ligands and GqDNA can occur through a complex pathway on a rugged energy landscape, where the reactants first come together to form an intermediate encounter complex – a pathway that is governed mainly by the diffusion-controlled association and dissociation rates (k_d and k_{-d}) of individual reactants (see figure 1). There might be a possibility of departure of these diffusing reactants from this intermediate encounter complex, but some of them can react to form a stable ligand/GqDNA complex through non-covalent interactions, which is mediated by the reaction controlled forward and backward reaction rates (k_r and k_{-r}) (figure 1). Since such ligand/GqDNA interactions typically occur at fast timescales which is of the order of tens to hundreds of microseconds, it is rather difficult for the existing real-time experimental methods like surface plasmon resonance (SPR) or stopped-flow measurements to track these very fast reaction rates accurately due to their limited time-resolution [79, 80]. Hence, we adopted FCS, whose time resolution can go down to picoseconds. Using FCS we collected the correlation of fluorescence fluctuations of the ligand (CV), arising from the ligand's diffusion in-and-out of a very small observation volume (~fl) and interaction with GqDNA during their dwell time within the observation volume. Applying appropriate model functions, we extracted the kinetic parameters from the reaction coupled diffusive correlation curves. From the steady state fluorescence quenching experiments of CV with varying concentrations of GqDNA, we found a reduction in the binding affinity of CV to antiparallel-GqDNA in the presence of 20% (w/v) glucose, sucrose and ficoll 70, as compared to that in pure buffer solution. The binding affinity of CV to antiparallel-GqDNA decreases by ~3 fold in the presence of the larger-sized crowder ficoll 70. Utilizing the steady state and FCS data, we obtained the quantitative information of all the reaction rates and found a gradual decrease in the overall association rates (k_+) as we go from pure buffer to 20% (w/v) ficoll 70. However, the overall dissociation rates remain nearly unchanged for smaller glucose and sucrose crowders, albeit a small increase in the dissociation rate is observed in the presence of ficoll 70. This decrease in overall association of CV to GqDNA is found to be mainly controlled by the diffusive reaction rates, k_d and k_{-d} as well as the decrease in the reaction controlled forward reaction rate k_r. Conversely, the reaction-controlled dissociation rates, k_{-r} (the rate-determining step) nearly remain unchanged in presence of the smaller crowders, but show a marginal increase in the presence of bigger ficoll 70, although the error bars of these extracted values remain high. This study, in continuation to our previous study [44] confirms that the chemical properties and/or size of saccharide crowders affect the ligand binding affinity to a groove of antiparallel-GqDNA, akin to the π-π

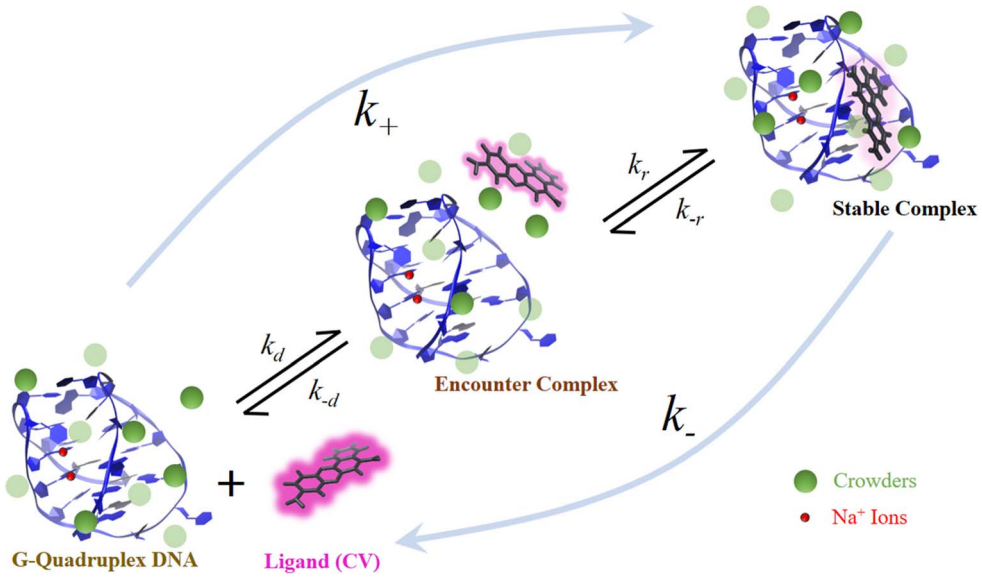

Figure 1. Scheme depicting the ligand (CV) and GqDNA interaction kinetics in the presence of crowders. The ligand/GqDNA complex formation occurs where the reactants (ligand and GqDNA) diffuse freely to interact with each other to form an intermediate encounter complex which is controlled by the diffusive rate constants (k_d and k_{-d}). This is followed by tight binding of the ligand with GqDNA through groove binding, mediated by reaction-controlled rate constants rates (k_r and k_{-r}). All these rate constants define the overall association and dissociation rates, k_+ and k_-.

stacking interactions of same ligand with the (3+1) hybrid GqDNA. Such interaction kinetics are mainly controlled by the viscosity-induced deceleration of the association rates, while the dissociation rate is less affected by these crowders. These results suggest that the crowders induce analogous effects on ligand/GqDNA complex formation in both situations where the ligand binding mode and the topology of GqDNA are changed. Although, the degree of this impact differs based on the ligand's intrinsic binding affinity for GqDNA of different structures, the underlying mechanism of interaction seems to remain remarkably similar. This holds true regardless of the ligand's mode of interaction; groove binding to antiparallel-GqDNA or π-π stacking interactions to (3+1) hybrid GqDNA.

2. Results and discussion

2.1. Circular dichroism data show no effect of crowders on structure of antiparallel-GqDNA

Circular dichroism (CD) spectroscopic analysis validates the formation of a basket-type antiparallel-GqDNA structure of 22-mer human telomeric DNA sequence, 5′-$AG_3TTAG_3TTAG_3TTAG_3$–3′ in the presence of 100 mM NaCl (see Supplementary material for methods and materials). The CD spectra of antiparallel-GqDNA in absence and presence of the crowders are shown in figure 2. The characteristic spectral signatures are evident, with two positive peaks at ~250 nm and ~295 nm, accompanied by a well-defined negative peak at ~265 nm, consistent with previous observations comfirming the formation of antiparallel-GqDNA [45]. Importantly, the addition of all three saccharide crowders does not induce any significant perturbation to the overall antiparallel-GqDNA topology. However it was found earlier that higher molecular weight saccharide crowder ficoll 70 marginally affects the (3+1) hybrid GqDNA structure [44]. This finding suggests that at physiologically relevant concentrations, these saccharide crowders likely have minimal impact on the antiparallel-GqDNA structure. This observation may also translate to the cellular milieu, as similar results were obtained when using Xenopus laevis egg extract, a complex crowding agent that mimics the crowded intracellular environment [78].

2.2. Reduction in binding strength of ligand to antiparallel-GqDNA in presence of crowders

The crowded cellular milieu is characterized by the presence of a diverse range of biomolecules, encompassing both small- and macro-molecules. The investigation of ligand binding to GqDNA in solution should ideally incorporate these ubiquitous crowders, as their presence can demonstrably influence the observed stability and binding affinity of the ligands [44, 51, 52, 63]. The small benzophenoxazine-core based ligand, CV investigated here displays intriguing fluorescence properties. In solution, CV exhibits high fluorescence intensity, however, upon complexation with GqDNA its fluorescence is efficiently quenched [45]. Notably, benzophenoxazine derivatives have been found to down-regulate the c-KIT expression in gastric cancer cells when binds with GqDNA, suggesting their potential as therapeutic agents [33]. Our previous study explored the CV binding with (3+1) hybrid GqDNA structure in the presence of saccharide crowders [44], however it is still unknown how

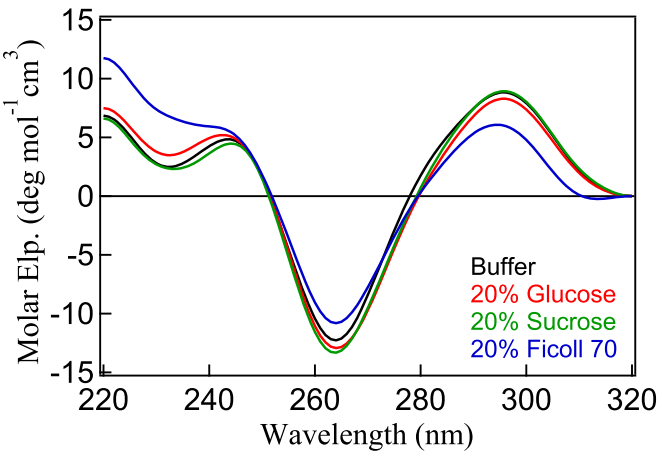

Figure 2. CD spectra of antiparallel-GqDNA formed by 22-mer human telomeric DNA sequence in the presence of Na^+ ions, as well as in the absence and presence of 20% (w/v) glucose, sucrose and ficoll 70. Data show typical signature of formation of antiparallel-GqDNA structure in all conditions. It is observed that glucose, sucrose and ficoll 70 do not affect the antiparallel-GqDNA structure.

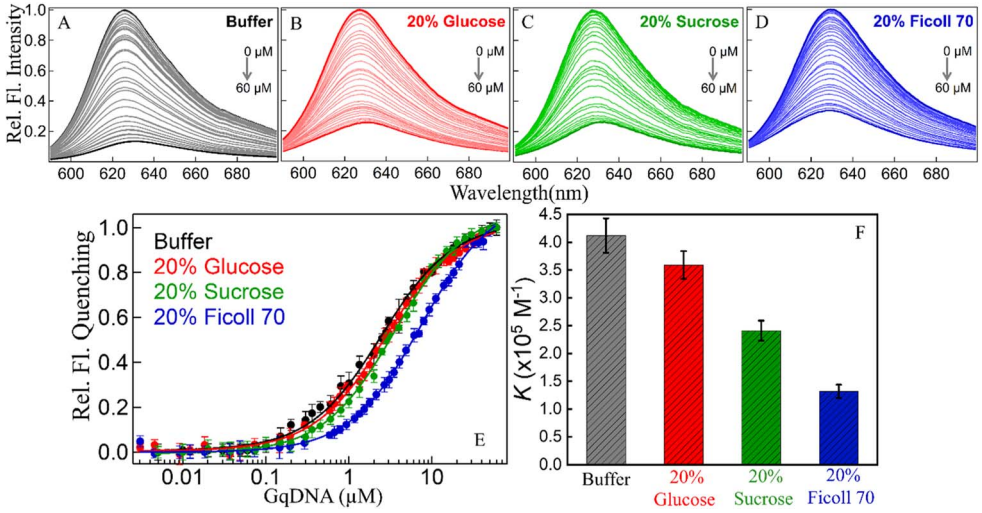

Figure 3. Relative quenching of fluorescence spectra of CV with increasing concentration of antiparallel-GqDNA in (A) buffer, (B) 20% (w/v) glucose, (C) 20% (w/v) sucrose and (D) 20% (w/v) ficoll 70. (E) The relative fluorescence quenching with GqDNA concentration, along with fits using equation S1. (F) Bar-graphs plotting the measured binding constants of CV to GqDNA from the fits to data in (E), in the absence and presence of the crowders. Error bars are obtained from triplicate measurements.

saccharide crowders affect the interaction between CV and antiparallel-GqDNA in its groove binding mode. The highly fluorescent state of CV gets quenched upon groove binding with GqDNA due to efficient electron transfer from electron rich guanines to the electron deficient CV [45]. We have kept the concentration of CV constant at ∼10 nM and performed a titration series by varying the concentration of preformed antiparallel-GqDNA up to 60 μM. It can be seen from figure 3 that the relative fluorescence intensity of CV, peaked at ∼626 nm, decreases gradually with the addition of GqDNA in pure buffer solution as well as in the presence of 20% (w/v) glucose, sucrose and ficoll 70 (figure 3(A)–(D)). However, the extent of quenching in all the cases are found to differ from each other which may arise from the induced local soft interactions of the crowder molecule that hinders the rate of electron transfer from guanines to CV. By analysing the graph of relative fluorescence quenching versus concentration of GqDNA and by fitting the binding curve with equation S1 (figure 3(E)), we found the binding constants (K) of CV with GqDNA in the absence and presence of glucose, sucrose and ficoll 70 differ appreciably which are plotted in a bar-graph in figure 3(F) and tabulated in table 1. This data reveals a modest alteration in the binding constant upon introduction of glucose and sucrose. However, a more substantial decrease is observed in the presence of ficoll 70, with binding constants diminishing by roughly 3-fold, as compared to that in pure buffer. These findings corroborate prior observations, where binding strength of small ligands with DNA in presence of crowding conditions drastically decreases [44, 63, 75]. Interestingly, the extent of the decrease in

Table 1. Binding constants of CV with antiparallel-GqDNA structure obtained from data in figure 3(E) at different crowding conditions.

Systems	Binding constant K ($\times 10^5$ M^{-1})
CV/GqDNA in Buffer	4.12 (±0.31)
CV/GqDNA in 20% Glucose	3.59 (±0.25)
CV/GqDNA in 20% Sucrose	2.41 (±0.18)
CV/GqDNA in 20% Ficoll 70	1.32 (±0.12)

binding affinity for CV to antiparallel-GqDNA is less pronounced as compared to that observed with (3+1) hybrid GqDNA [44].

To isolate the effect of GqDNA binding on the fluorescence properties of CV, we also measured control spectra of CV in the presence of crowders only (in the absence of GqDNA) as well as monitored the interaction of Cy3-labeled-GqDNA with ficoll 70 (see supplementary materials). This step aimed to determine if the observed fluorescence quenching stemmed primarily from ligand interaction with the antiparallel-GqDNA groove or induced by the crowders, or if there is any direct interaction of bigger crowder (ficoll 70) and the GqDNA. Interestingly, we observed that there is as such no interaction occurs between the GqDNA and ficoll 70, as exemplified by the nearly unchanged fluorescence spectra of Cy3-GqDNA in the presence of varying concentration of ficoll 70 (see supplementary materials, figure S2). However, ∼2-fold enhancement in the fluorescence signal of CV is observed upon addition of the crowders in the absence of GqDNA (figure S3A), in contrast to much stronger quenching (∼5 fold) of CV fluorescence upon binding to GqDNA (figure 2(A)). This phenomenon can be attributed to changes in the surrounding environment, induced by the crowders, possibly due to variations in dielectric constant and/or viscosity and/or weak interaction of CV with crowders. These compelling observations suggest that the relatively higher quenching of CV fluorescence observed above is mainly linked to its groove binding interaction with antiparallel-GqDNA, potentially facilitating electron transfer from guanine residues to the ligand molecule. This is also because, we performed fluorescence titration of CV (10 nM) with varying concentration of the biggest crowder, ficoll 70 in the absence of GqDNA and found that the binding of CV to ficoll 70 alone is much weaker (∼10^2 M^{-1}, see figure S3B), as compared to that observed for CV binding to GqDNA in the presence of crowders (∼10^5 M^{-1}, see table 1).

Notably, x-ray crystallographic study by Neidle and co-workers unraveled that there is one groove, which is long and narrow, contains stable spine-of-hydration within antiparallel-GqDNA, which is equivalent to, but structurally different than those found in the minor groove of duplex-DNA [81]. Even though it is documented that binding of ligands such as TMPyP4, BMVC, Hoechst 33258, etc to quadruplex DNA accompany re-arrangement of groove-bound water molecules [52, 82], it is not known how crowding agents may actually affect the binding affinity of ligands, disturbing such spine-of-hydration within the groove of antiparallel-GqDNA. The above steady-state fluorescence data of CV binding to human telomeric antiparallel-GqDNA clearly show that there are local effects on the destabilization of the ligand binding inside the groove of GqDNA by the saccharide crowders, where the re-arrangement of groove-bound water may play a crucial role.

2.3. Fluorescence correlation spectroscopy (FCS) data

2.3.1. Determination of the kinetic parameters of CV/GqDNA interactions

The involvement of both diffusion and reaction kinetics in the ligand/GqDNA interactions make it difficult to get the quantitative information of individual reaction rates because of their very fast and broad timescale [44–47]. Although one can measure the overall binding constant of ligand to GqDNA by using the real time experimental techniques (like SPR, stopped-flow method, etc) the time resolution of which can only go down to ∼1 ms [46, 79, 80, 83]. Hence, measuring the association and dissociation processes which occur in tens-to-hundreds of microseconds time-scale become difficult using these real-time techniques. So, to gather the quantitative knowledge of the molecular processes occurring in the faster time-scales, we used a home-built FCS setup which uses a laser beam that under-fills the back-aperture of a high numerical aperture objective to create a large confocal volume, such that reaction and diffusion correlations remain separated in time [44–47]. In FCS, a tiny observation volume (∼fl) is created by the tight focusing of a laser beam inside the sample and then fluorescence fluctuations from a probe are correlated, which arise from the ON and OFF state of the probe molecule due to its diffusion in-and-out of the observation volume or due to any chemical reaction that changes the fluorescence state of the probe [44–47]. From these correlation curves, one can extract the information about diffusion and reaction rates of the interaction of the fluorescent as well as non-fluorescent molecules with GqDNA [44–47].

Previously, the ligand induced equilibration of unstructured and unfolded form of GqDNA towards the equilibrated folded conformations were investigated through FCS measurements [84]. FCS has important applications in exploring the photo-induced charge transfer and charge recombination processes in DNA from the fluorescence blinking of ligands [85], pH-dependent topological alteration of i-motif DNA [86], discernment of Watson-Crick base-pairs from the damaged ones by the auto-flipping dynamics of the mismatched bases [87]. It can probe the structural changes in proteins [56, 57, 88–92] along with a special ability to distinguish between the

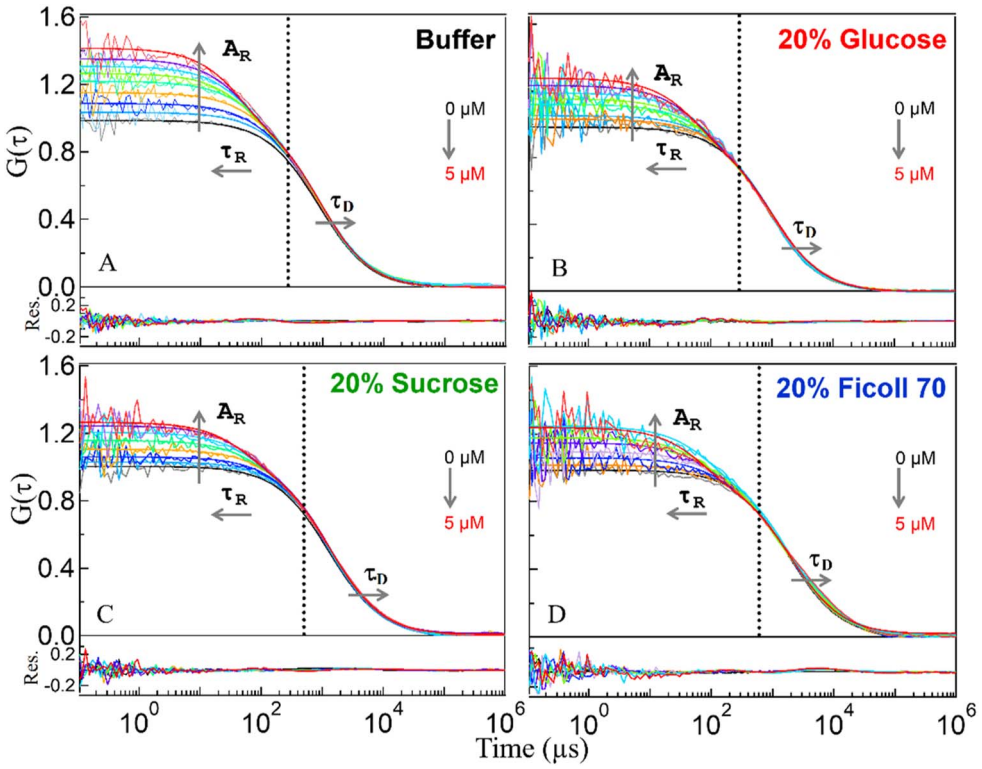

Figure 4. Normalized fluorescence correlation curves of CV with varying concentrations of antiparallel-GqDNA in (A) buffer, (B) 20% w/v glucose, (C) 20% w/v sucrose and (D) 20% w/v ficoll 70. Plots also include the (global) fits to the data-sets using equation (3), along with the residuals-of-fits. The correlation data show typical characteristics of GqDNA concentration dependent change of reaction-time, reaction-amplitude and diffusion time. See figure S2 for the variation of reaction time and amplitude and table 2 for the estimated kinetic parameters.

normal and hyperactivated Ras-signaling in pathogenic fungal-membranes [93]. This technique can measure the population of amyloid-protein aggregates [94, 95] and calculate the detailed kinetic rates of ligand-macromolecule interactions [44, 96]. Interestingly, FCS can also gauge the size distribution and polydispersity factors of microemulsion droplets (MEDs) in solutions and predict the formation kinetics of nanorods inside the microemulsion droplets (MEDs) in a step-wise manner, just to mention a few [97–99].

Using our home-built dual channel FCS setup, we excited the CV/GqDNA samples by a 532 nm laser beam in an under-filled objective back-aperture which creates a large confocal volume to well separate the diffusion and reaction components in time [44–46]. To work at a (near) single molecule level, very low concentration (<1 nM) of the fluorescent ligand (CV) was taken, while we varied the concentration of GqDNA from zero to 5 μM and collected the reaction-coupled diffusion correlation curves in the absence and presence of 20% (w/v) of glucose, sucrose and ficoll 70. Figure 4 plots the GqDNA concentration dependent correlation curves for each of these CV/GqDNA systems in the absence and presence of crowders, along with their fits. The distinct features can be seen from the correlation curves in which the diffusion dynamics occurring above ~600 μs, whereas the CV/GqDNA interactions kinetics arise below ~600 μs. Interestingly, we found that as the concentration of GqDNA is increased, there is slowing down of diffusion time of the CV/GqDNA complex as well as swift in the reaction time. This suggests a rise in the formation of the complex in solution with increasing concentration of GqDNA [45]. There is also a rise in reaction amplitude of the CV/GqDNA interaction as we increase the concentration of GqDNA [45]. In presence of all the crowders taken here, the pattern of the correlation curves remains similar except some decrease in the extent of reaction amplitude change as well as the increase of diffusion of the complex due to the varied viscosity induced by the different crowders.

Assuming the formation of the stable CV/GqDNA complex to be a single-step biomolecular reaction where the degree of interaction between CV and GqDNA is controlled mainly by the association (k_+) and dissociation (k_-) rates, the interaction can be interpreted as,

$$\mathrm{CV} + \mathrm{GqDNA} \underset{k_-}{\overset{k_+}{\rightleftharpoons}} \mathrm{CV-GqDNA} \tag{1}$$

The binding strength is then quantified by the equilibrium binding constant (K) of CV with GqDNA which is defined as the ratio of k_+ to k_- i.e.,

$$K = \frac{k_+}{k_-} \tag{2}$$

We have performed a global data analysis of the above correlation curves obtained from FCS measurements by using the following equation which takes care of the molecular events like diffusion and reaction of CV with GqDNA when they pass through the small observation volume [45, 46, 96].

$$G(\tau) = \frac{1}{\langle N \rangle}\left(1 + \left(\frac{\tau}{\bar{\tau}_D}\right)\right)^{-1} \times \left[1 + s\left(\frac{\tau}{\bar{\tau}_D}\right)\right]^{-1/2}[1 + A_R e^{-\frac{\tau}{\tau_R}}] \tag{3}$$

Here, $\langle N \rangle$ is the average number of ligands (CV) within the observation volume, $\bar{\tau}_D$ is the average time th CV or CV/GqDNA complex takes to diffuse through the observation volume, s is instrument correction factor, A_R is reaction amplitude and τ_R is the reaction time that can be written in terms of the rate constants as [45, 46, 96],

$$\tau_R = \frac{1}{k_+[GqDNA] + k_-} = \frac{1}{k_-(1 + K[GqDNA])} \tag{4}$$

In the global fitting analysis, s was set as a fixed global parameter, whereas $\bar{\tau}_D$, A_R and τ_R were the GqDNA concentration dependent free parameters (see figure S4 in supplementary materials for the GqDNA concentration dependent variations of A_R and τ_R). In our previous work, we successfully employed the modified equation including a stretched factor (β) in the reaction time, τ_R to analyse FCS data for the CV/(3+1) hybrid GqDNA system [44]. However, this approach is not directly applicable here. Unlike the (3+1) hybrid structure where CV binds to the G-tetrad in various orientations through π-π stacking interaction, the current study focuses on an antiparallel-GqDNA structure where CV binds specifically to the groove and one may not expect to observe the different orientation of the ligand bound to such narrow groove created by antiparallel-GqDNA. In fact, use of such stretched factor (β) in equation (3) did not improve the fitted results, suggesting a single mode of groove-binding of CV to antiparallel-GqDNA.

Table 2 summarizes the association (k_+) and dissociation (k_-) rate constants obtained from the FCS data for CV/GqDNA interactions in the absence and presence of crowders. A key observation from this dataset is that the crowder-induced decrease in binding constants is primarily attributed to a deceleration of the association rate constant (k_+). This k_+ value exhibits a nearly three-fold decrease upon transitioning from pure buffer to a 20% ficoll 70 solution. Interestingly, the dissociation rate constants (k_-) remain largely unaffected across all conditions, except a very small increase (~1.1 times) in the presence of ficoll 70. These findings align well with our previous observations, where a more pronounced decrease (approximately five-fold) in the association rate constant of CV to hybrid GqDNA structure was observed in presence of ficoll 70 [44]. It is noteworthy that in our earlier study with the (3+1) hybrid GqDNA, CV interacted via a stronger π-π stacking interaction with the G-tetrads, compared to the groove binding observed here with the antiparallel-GqDNA. This suggests that regardless of the distinct binding modes (π-π stacking versus groove binding) employed by CV for (3+1) hybrid and antiparallel-GqDNA, the crowders mainly produce the viscosity-induced deceleration of association rate to control the overall binding affinity of the ligand to GqDNA, with minimally impacting the ligand dissociation rates for both GqDNA structures.

These findings present a unique perspective on ligand/GqDNA interactions within crowded environments. Notably, these results suggest that once a ligand establishes a binding site with GqDNA (be it antiparallel or hybrid conformation [44]), through either rapid or slower association, the presence of differently sized crowders exerts minimal influence on the ligand/GqDNA complex itself to induce the ligand dissociation rates. This observation is manifested in the negligible impact of crowders on the activation barrier for ligand dissociation. While the overall binding affinity of the ligand to GqDNA is demonstrably decreased, the dissociation process appears remarkably unaffected by the crowded environments, especially in the presence of smaller crowders, albeit a minimal effect exerted by the much bigger ficoll 70 crowder. Since the volume exclusion or the overall steric factor induced by all the three crowders at 20% (w/v) concentration remains almost similar [76, 77], the above effects might be originating from the local interactions of crowders with the CV/GqDNA complex [76, 77].

2.3.2. Regulation of binding strength of ligand to GqDNA by viscosity-induced diffusive and reaction-controlled forward kinetic rate constants

The reduction in the binding affinity of CV with GqDNA in the presence of crowders as compared to that in pure buffer solution is mainly governed by the fall in association rates, k_+. To know quantitatively how these association and dissociation rates are affected directly by the crowders, we assumed these interactions to occur in a three-state model where the interacting entities come closer to each other to form an intermediate encounter complex which is governed mainly by diffusion of reacting species (k_d and k_{-d}). In the solvation shell of GqDNA, CV binds in the groove to form the final stable CV/GqDNA complex which is regulated by the reaction-controlled forward (k_r) and reverse (k_{-r}) reaction rates (see figure 1).

With a prior knowledge of the size (hydrodynamic radii) and diffusion constants of both ligand and GqDNA which are obtained from the FCS measurements (see supplementary material), the Smoluchowski equation gives an expression for diffusion-

Table 2. Ligand binding and kinetic parameters estimated from steady-state fluorescence and FCS measurements for CV/antiparallel-GqDNA interactions.

System CV/GqDNA	K ($\times 10^5\,M^{-1}$)	k_+ ($\times 10^9\,M^{-1}s^{-1}$)	k_- ($\times 10^3\,s^{-1}$)	k_d ($\times 10^9\,M^{-1}s^{-1}$)	k_{-d} ($\times 10^9\,s^{-1}$)	K_{enc} (M^{-1})	k_r ($\times 10^9\,s^{-1}$)	k_{-r} ($\times 10^3\,s^{-1}$)	K_{reac} ($\times 10^5$)
In Buffer	4.12 (±0.31)	3.19 (±0.29)	7.75 (±0.41)	11.67 (±0.72)	0.94 (±0.09)	12.41 (±1.41)	0.35 (±0.06)	10.61 (±2.23)	0.33 (±0.04)
In 20% Glucose	3.59 (±0.25)	2.33 (±0.24)	6.50 (±0.50)	5.66 (±0.56)	0.46 (±0.06)	12.30 (±2.01)	0.32 (±0.08)	11.03 (±3.35)	0.29 (±0.05)
In 20% Sucrose	2.41 (±0.18)	1.96 (±0.21)	8.12 (±0.61)	5.60 (±0.52)	0.45 (±0.05)	12.44 (±1.80)	0.24 (±0.05)	12.63 (±3.30)	0.19 (±0.03)
In 20% Ficoll 70	1.32 (±0.12)	1.10 (±0.12)	8.60 (±0.48)	1.99 (±0.18)	0.16 (±0.02)	12.44 (±1.92)	0.20 (±0.06)	18.18 (±6.38)	0.11 (±0.02)

controlled association rate (k_d) as [100],

$$k_d = 4\pi(D_{CV} + D_{GqDNA})(Rh_{CV} + Rh_{GqDNA})N_{av} \quad (5)$$

Where, D_{CV} and D_{GqDNA} are the diffusion coefficients and Rh_{CV} and Rh_{GqDNA} are the hydrodynamic radii of the ligand (CV) and GqDNA, respectively, and N_{av} is the Avogadro number.

To account for the effects of crowding on ligand/GqDNA interactions, the solution (micro) viscosity was determined in the presence of various crowding agents using the diffusion time of standard Rh6G in water as a viscosity reporter (see figure S5 in the supplementary material). Subsequently, the size (hydrodynamic radius) of the ligand was assessed using Rh6G as a reference standard (see figure S6 in the supplementary material). By leveraging the solution viscosity data, the diffusion constants of CV were calculated for each crowder condition. The size of the antiparallel-GqDNA was obtained from prior sedimentation experiments [101]. This value, along with the Stokes-Einstein equation, was then employed to calculate the diffusion constant of antiparallel-GqDNA in the presence of crowders. In this case we assumed that the size (R_h) of GqDNA does change in respective crowder solutions, which is also suggested by the CD measurements showing a no change in the topology of antiparallel GqDNA (see figure 2). By using the values of diffusion coefficients and sizes (table S1 in supplementary materials) of the ligand and GqDNA in respective solutions, k_d values are calculated from equation (5) and tabulated in table 2 for each systems.

For the dissociation of the ligand from the biomolecules, the ligand and GqDNA should diffuse apart from each other by a minimum distance equal to the size of the complex. From the time taken by the ligand and biomolecule to diffuse apart the minimum distance, one can calculate the dissociation rate (k_{-d}) of encounter complex. Thus, the equilibrium binding constant of the encounter complex ($K_{enc} = k_d/k_{-d}$) can be modelled as the volume occupied by the ligand and GqDNA [96]. Hence one can write,

$$k_{-d} = \frac{k_d}{\pi(Rh_{CV} + Rh_{GqDNA})^3 N_{av}} = \frac{4(D_{CV} + D_{GqDNA})}{(Rh_{CV} + Rh_{GqDNA})^2} \quad (6)$$

Among many intermediate encounter complexes, some of them can form a stable (inclusion) complex which is regulated by the reaction-controlled forward (k_r) and reverse (k_{-r}) reaction rates (see figure 1). So, the equilibrium constant for the formation of this stable complex can be written as,

$$K_{reac} = \frac{k_r}{k_{-r}} \quad (7)$$

Separating the whole equilibrium process into a pre-equilibrium between the freely diffusing species and the encounter complex as well as an inclusion equilibrium between the encounter complex and final stable complex, we can write the overall binding constant, $K = K_{enc} \times K_{reac}$. With the steady state assumption, we have calculated the binding constants of all the systems at equilibrium. Expressing the binding constant, $K = K_{enc} \times K_{reac}$ and utilizing the values of binding constants (K) and diffusion limited equilibrium constant of encounter complex, K_{enc} as ~12.4 M^{-1} (see table 2), the K_{reac} is found to be in the order of ~10^4 for all systems studied here, which clearly suggest that the forward rate(k_r) for the stable complex formation is much higher than the dissociation rate (k_{-r}) of the ligand from the complex. This must be the case as the calculated binding constants are in the order of ~10^5 M^{-1}, which means the ligand spend most of its time in bound state, suggesting the dissociation rate (k_{-r}) to be much smaller, as compared to the other rates, which is the main rate determining step. Thus, for a very low unbinding rate (k_{-r}) of the ligand from the stable complex which is formed by the groove binding of ligand to GqDNA, the faster reaction-controlled association rates can be expressed as [96].

$$k_r = \frac{k_+ \times k_{-d}}{k_d - k_+} \quad (8)$$

From the table 2 and figure 5 which include the quantitative values of all the rate constants and their bar-graph representations, respectively, the ~3 times decrease in the binding constant of CV to GqDNA in the presence of ficoll 70 in comparison to that in pure buffer is attributed mainly to the reduction of association (k_+) rates. The changes in this overall k_+ are controlled by the diffusive (k_d and k_{-d}) and reaction-controlled forward rate k_r. The monotonous decrease in the overall association rate (k_+), as we go from pure buffer to 20% (w/v) of ficoll 70, is mainly due to the gradual decrement in both the diffusion-controlled rates (k_d and k_{-d}) and reaction-controlled forward rate (k_r). However, there is effectively no change in the overall dissociation (k_-) for the smaller glucose and sucrose crowders, which is the rate determining step of the interaction; however, a small increment in the dissociation rate is observed in case of higher molecular weight ficoll 70 crowders (see figure 5(H)). Although there is a significant fall in k_d and k_{-d} values, their ratio ($K_{enc} = k_d/k_{-d}$) which is the equilibrium constant of formation of the intermediate encounter complex, does not change in presence of the crowders in comparison to that in dilute solution. So, even if there is viscosity-induced reduction in the individual diffusion-controlled kinetic rates, their equilibrium constant remains similar (see figure 5(F)). The rates governing the formation of the final stable complex from the pre-equilibrated encounter complex, the reaction-controlled association (k_r) decrease as one transit from dilute condition to that in ficoll 70. Conversely, there is effectively no change in the reaction-controlled dissociation rates (k_{-r}, the rate-determining step) in the presence of

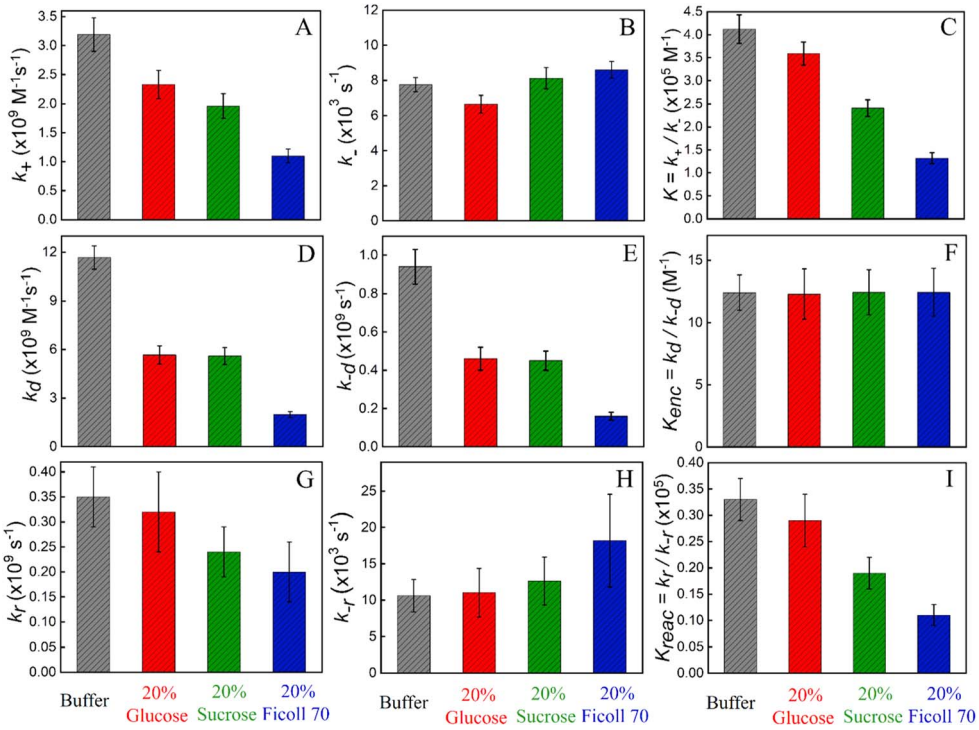

Figure 5. Bar-graphs showing the relative changes of the kinetic parameters; (A) k_{+}, (B) k_{-}, (C) k_{+}/k_{-}, (D) k_{d}, (E) k_{-d}, (F) K_{enc}, (G) k_{r}, (H) k_{-r}, (I) K_{reac} obtained from the FCS measurements. Data show that the diffusion-controlled association rates are the dominating factors which are modulated by the crowder-induced viscosity change. The dissociation rates of the ligand from the stable complex remain nearly unchanged in the presence of the smaller sized crowders, with slight increment observed in the presence of ficoll 70. The error bars were obtained from triplicate sets of data.

smaller sized crowders. However, in the presence of the higher branched molecular crowder ficoll 70, we observe a slight increase in the k_{-r}. This increment may arise from ficoll 70 coming into closer proximity of CV and interacting with it when it is bound within the groove of the antiparallel-GqDNA structure. In fact, the binding constant of CV to ficoll 70 in the absence of GqDNA has been found to be $\sim 10^{2}\ M^{-1}$ which is much lower than those of CV binding to GqDNA ($\sim 10^{5}\ M^{-1}$) in the presence of the crowders. Although, the strength of interaction of CV/ficoll 70 is much smaller than that of CV/GqDNA, the ficoll may still influence the unbinding rates of the ligand through soft local interactions. However, the nature and origin of this soft interaction needs further investigations. This phenomenon was not observed in the earlier study where CV bound to the G-tetrad via π-π stacking interaction in the (3+1) hybrid structure [44]. Collectively, these observations suggest that the chemical properties and/or size of the (saccharide) crowders do not modulate the groove binding interaction between CV and antiparallel-GqDNA, except mildly by the branched ficoll 70 crowder. The stark contrast between the significant alteration in k_{r} and the relatively unaltered k_{-r} translates to a decrease in the equilibrium constant ($K_{reac} = k_{r}/k_{-r}$) for the formation of the final stable complex with increasing crowder size. Similar trends were observed in our previous study, albeit with a more pronounced effect [44]. This implies that these crowders exert comparable effects in both the scenarios, irrespective of whether CV interacts via groove binding to antiparallel-GqDNA or π-π stacking interactions with (3+1) hybrid GqDNA structures [44].

Previous stopped-flow study showed the viscosity-driven retardation in the association of ssDNA and cold shock protein B (CspB) to be independent of the crowders, whereas the dissociation rates depend strongly on the size and chemical nature of the crowders [60]. Another exciting study by Schuler and co-workers unravelled the effect of molecular crowding on the interaction between two intrinsically disordered proteins (IDPs) [62]. They considered the size and concentration dependencies of ethylene glycol and its polymers of different molecular weights on the folding/unfolding dynamics of two IDPs by employing single molecule Förster resonance energy transfer (smFRET) technique [62]. At higher concentration range (typically, more than 100 mg ml^{-1} or 10% (w/v) of all the crowders), they found a viscosity-induced deceleration of the association rates, as well as a depletion-induced acceleration of the association of the interacting IDPs in the lower concentration ranges which was predominant in the case of PEGs of higher molecular weights [62]. In our recent investigation, we elucidated the impact of mono- and polysaccharide crowders, including glucose, sucrose, and ficoll 70, on the binding affinity of CV with (3+1) hybrid GqDNA. These small and macromolecular crowders were

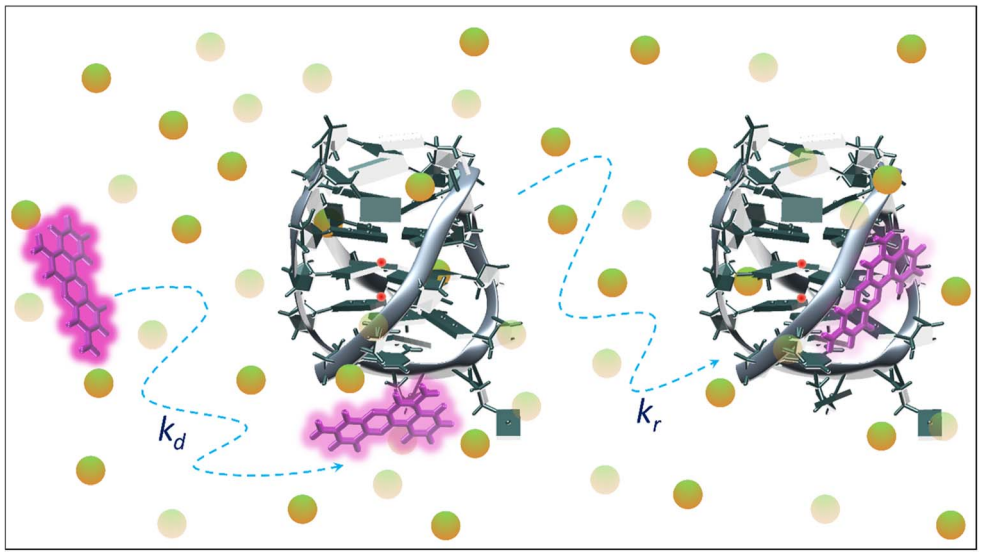

Figure 6. Cartoon showing the diffusion-controlled association which forms the (intermediate) encounter complex where the ligand comes within the solvation shell of GqDNA, followed by the association of ligand into the groove binding-mode with antiparallel-GqDNA.

observed to modulate the extent of ligand binding through a viscosity-induced deceleration of association rates. Importantly, the dissociation rate constant of the CV/hybrid GqDNA complex remained relatively unperturbed, signifying the preservation of complex stability in the presence of these crowders [44]. The present findings regarding viscosity-driven effects demonstrate a significant concordance with prior observations, particularly at higher crowder concentrations of 20% (w/v). However, further exploration is necessary to gain a deeper understanding of the intriguing phenomena associated with depletion effects exerted by these crowders at lower concentration regimes. Interestingly, our data consistently revealed that irrespective of the distinct binding modes employed by CV, i.e., π-π stacking with (3+1) hybrid GqDNA [44] and groove binding with antiparallel-GqDNA (present study), the saccharide crowders exhibit minimal influence on ligand dissociation from the GqDNA structures. The overall decrease in binding affinity of ligand to GqDNA in presence of different molecular weight saccharide crowders is mainly controlled by the viscosity-induced deceleration of association rates, given that the overall volume exclusion and steric effects exerted by all three saccharide crowders used here remain similar. These results suggest that the crowders can affect the viscosity-induced changes in the ligand association to GqDNA, but their effects on the unbinding of the ligand from antiparallel-GqDNA remain minimal, similar as observed earlier for π-stacking interaction of ligand with hybrid GqDNA structure [44]. A cartoon showing the possible ligand diffusion and subsequent association with GqDNA is presented in figure 6.

3. Conclusion

There are several in vitro as well as in silico studies available on the thermodynamic aspects of ligand/GqDNA interactions in the absence and presence of different macromolecular crowders that mimic the cell-like environments. However, the detailed estimation of all the kinetic rates that control the ligand binding affinity with GqDNA in absence and presence of different molecular crowders remained sparse till date. Our current study focused on the various kinetic parameters that affect the binding of a benzophenoxazine-core based ligand, cresyl violet (CV) with the human telomeric antiparallel-GqDNA structure in the absence and presence of macromolecular crowders like glucose, sucrose and ficoll 70 at a physiological crowder concentration. Using our home-built FCS setup, aided by other spectroscopic techniques, we calculated all the diffusion as well as reaction-controlled kinetic rates of CV/antiparallel-GqDNA interaction in the absence and presence of crowders at a (near) single molecule level. Our prior investigations have focused on elucidating the effects of saccharide crowders on the kinetic parameters associated with the interaction between CV and hybrid GqDNA. The current study extends this knowledge base by experimentally demonstrating that these same crowders modulate the binding affinity of CV towards antiparallel-GqDNA. This modulation is predominantly attributed to a viscosity-induced decrease in the association rate constant (k_+). Interestingly, the dissociation rate constant (k_-) remains largely unaffected, mirroring observations from our previous work on (3+1) hybrid GqDNA, albeit with a more pronounced effect. These findings compellingly suggest that the crowders exert comparable influences on the ligand/GqDNA

interaction kinetics irrespective of the distinct binding modes employed by CV with GqDNA i.e. groove binding with antiparallel-GqDNA versus π-π stacking interactions with (3+1) hybrid GqDNA. To achieve a comprehensive understanding of how various molecular crowders influence ligand/GqDNA binding interactions, further in vitro studies employing advanced spectroscopic techniques are essential. Additionally, in silico investigations utilizing enhanced sampling methods can provide valuable insights into the underlying molecular mechanisms governing these interactions. This work, in conjunction with our prior study serves as a foundational steps towards a more comprehensive exploration of ligand binding/unbinding processes with GqDNA within crowded environments. Elucidating the key mechanistic parameters that direct these interactions holds significant potential for the rational scheme and development of possible antitumour drugs which may target the GqDNA structures in real cellular crowded environment.

Acknowledgments

This work is supported by SERB project granted to S S (CRG/2018/002238). CD data and some steady-state fluorescence data were measured in the Department of Chemistry, Indian Institute of Technology, Delhi (IITD), India. P A thanks UGC; A K C thanks JNU; M F K thanks CSIR for fellowships. We thank Souvik Maiti (IGIB Delhi) and Pramit K Chowdhury (IIT Delhi) for the access to instruments of fluorescence and CD measurements. The authors have declared that no conflicting interests exist.

Data availability statement

All data that support the findings of this study are included within the article (and any supplementary files).

ORCID iDs

Ajay Kumar Chand https://orcid.org/0009-0005-9089-3272
Sobhan Sen https://orcid.org/0000-0002-9047-3455

References

[1] Huppert J L and Balasubramanian S 2007 G-quadruplexes in promoters throughout the human genome *Nucleic Acids Res.* **35** 406–13
[2] Eddy J and Maizels N 2008 Conserved elements with potential to form polymorphic G-quadruplex structures in the first intron of human genes *Nucleic Acids Res.* **36** 1321–33
[3] Halder K, Halder R and Chowdhury S 2009 Genome-wide analysis predicts DNA structural motifs as nucleosome exclusion signals *Mol. Biosyst.* **5** 1703–12
[4] Burge S, Parkinson G N, Hazel P, Todd A K and Neidle S 2006 Quadruplex DNA: sequence, topology and structure *Nucleic Acids Res.* **34** 5402–15
[5] Spiegel J, Adhikari S and Balasubramanian S 2020 The structure and function of DNA G-quadruplexes *Trends Chem* **2** 123–36
[6] Sundquist W I and Klug A 1989 Telomeric DNA dimerizes by formation of guanine tetrads between hairpin loops *Nature* **342** 825–9
[7] Patel D J, Phan A T and Kuryavyi V 2007 Human telomere, oncogenic promoter and 5′-UTR G-quadruplexes: diverse higher order DNA and RNA targets for cancer therapeutics *Nucleic Acids Res.* **35** 7429–55
[8] Phan A T, Kuryavyi V, Burge S, Neidle S and Patel D J 2007 Structure of an unprecedented G-quadruplex scaffold in the human c-kit promoter *J. Am. Chem. Soc.* **129** 4386–92
[9] Neidle S and Parkinson G N 2003 The structure of telomeric DNA *Curr. Opin. Struct. Biol.* **13** 275–83
[10] Rhodes D and Lipps H J 2015 G-quadruplexes and their regulatory roles in biology *Nucleic. Acids Res.* **43** 8627–37
[11] Clynes D, Higgs D R and Gibbons R J 2013 The chromatin remodeller ATRX: a repeat offender in human disease *Trends Biochem. Sci.* **38** 461–6
[12] McEachern M J, Krauskopf A and Blackburn E H 2000 Telomeres and their control *Annu. Rev. Genet.* **34** 331–58
[13] Zhang M-L, Tong X-J, Fu X-H, Zhou B O, Wang J, Liao X-H, Li Q-J, Shen N, Ding J and Zhou J-Q 2010 Yeast telomerase subunit Est1p has guanine quadruplex-promoting activity that is required for telomere elongation *Nature Structural & Molecular Biology* **17** 202–9
[14] Robinson J, Raguseo F, Nuccio S P, Liano D and Di Antonio M 2021 DNA G-quadruplex structures: more than simple roadblocks to transcription? *Nucleic Acids Res.* **49** 8419–31
[15] Cogoi S, Paramasivam M, Spolaore B and Xodo L E 2008 Structural polymorphism within a regulatory element of the human KRAS promoter: formation of G4-DNA recognized by nuclear proteins *Nucleic Acids Res.* **36** 3765–80
[16] Kim N 2019 The Interplay between G-quadruplex and Transcription *Curr. Med. Chem.* **26** 2898–917
[17] Simone R, Fratta P, Neidle S, Parkinson G N and Isaacs A M 2015 G-quadruplexes: emerging roles in neurodegenerative diseases and the non-coding transcriptome *FEBS Lett.* **589** 1653–68
[18] David A P, Margarit E, Domizi P, Banchio C, Armas P and Calcaterra N B 2016 G-quadruplexes as novel cis-elements controlling transcription during embryonic development *Nucleic Acids Res.* **44** 4163–73
[19] Hou Y, Li F, Zhang R, Li S, Liu H, Qin Z S and Sun X 2019 Integrative characterization of G-quadruplexes in the three-dimensional chromatin structure. *Epigenetics* **14** 894–911
[20] Li L, Williams P, Ren W, Wang M Y, Gao Z, Miao W, Huang M, Song J and Wang Y 2021 YY1 interacts with guanine quadruplexes to regulate DNA looping and gene expression. *Nat. Chem. Biol.* **17** 161–8
[21] Sabari B R *et al* 2018 Coactivator condensation at super-enhancers links phase separation and gene control. *Science* **361**
[22] Boija A *et al* 2018 Transcription factors activate genes through the phase-separation capacity of their activation domains. *Cell* **175** 1842–1855.e16
[23] Rodriguez R, Miller K M, Forment J V, Bradshaw C R, Nikan M, Britton S, Oelschlaegel T, Xhemalce B, Balasubramanian S and Jackson S P 2012 Small-molecule-induced DNA damage identifies alternative DNA structures in human genes. *Nat. Chem. Biol.* **8** 301–10
[24] De Magis A, Manzo S G, Russo M, Marinello J, Morigi R, Sordet O and Capranico G 2019 DNA damage and genome instability by G-quadruplex ligands are mediated by R loops in human cancer cells. *Proc. Natl. Acad. Sci. U S A* **116** 816–25
[25] Tian T, Chen Y-Q, Wang S-R and Zhou X 2018 G-quadruplex: a regulator of gene expression and its chemical targeting *Chem.* **4** 1314–44
[26] Maizels N and Gray L T 2013 The G4 Genome *PLoS Genet.* **9** e1003468–1003468
[27] Burger A M, Dai F, Schultes C M, Reszka A P, Moore M J, Double J A and Neidle S 2005 The G-quadruplex-interactive molecule BRACO-19 inhibits tumor growth, consistent with telomere targeting and interference with telomerase function *Cancer Res.* **65** 1489–96

[28] Lin W et al 2013 Mammalian DNA2 helicase/nuclease cleaves G-quadruplex DNA and is required for telomere integrity. EMBO J. 32 1425–39
[29] Wolfe A L et al 2014 RNA G-quadruplexes cause eIF4A-dependent oncogene translation in cancer Nature 513 65–70
[30] Bugaut A and Balasubramanian S 2012 5'-UTR RNA G-quadruplexes: translation regulation and targeting Nucleic Acids Res. 40 4727–41
[31] Beaudoin J-D and Perreault J-P 2013 Exploring mRNA 3′-UTR G-quadruplexes: evidence of roles in both alternative polyadenylation and mRNA shortening Nucleic Acids Res. 41 5898–911
[32] Ahmed A A et al 2020 Asymmetrically substituted quadruplex-binding naphthalene diimide showing potent activity in pancreatic cancer models ACS Med. Chem. Lett. 11 1634–44
[33] McLuckie K I E, Waller Z A E, Sanders D A, Alves D, Rodriguez R, Dash J, McKenzie G J, Venkitaraman A R and Balasubramanian S 2011 G-quadruplex-binding benzo[a] phenoxazines down-regulate c-KIT expression in human gastric carcinoma cells J. Am. Chem. Soc. 133 2658–63
[34] Marchetti C et al 2018 Targeting multiple effector pathways in pancreatic ductal adenocarcinoma with a G-quadruplex-binding small molecule J. Med. Chem. 61 2500–17
[35] Xu H et al 2017 CX-5461 is a DNA G-quadruplex stabilizer with selective lethality in BRCA1/2 deficient tumours Nat. Commun. 8 14432
[36] Savva L and Georgiades S N 2021 Recent developments in small-molecule ligands of medicinal relevance for harnessing the anticancer potential of G-quadruplexes Molecules 26 841
[37] Santos T, Salgado G F, Cabrita E J and Cruz C 2021 G-quadruplexes and their ligands: biophysical methods to unravel G-quadruplex/Ligand Interactions Pharmaceuticals 14 769
[38] Asamitsu S, Yu T, Sugiyama H S and Obata Z B 2019 Recent progress of targeted G-quadruplex-preferred ligands toward cancer therapy Molecules 24 429–57
[39] Haider S M, Neidle S and Parkinson G N 2011 A structural analysis of G-quadruplex/ligand interactions Biochimie. 93 1239–51
[40] Chaires J B 2006 A thermodynamic signature for drug–DNA binding mode Arch. Biochem. Biophys. 453 26–31
[41] Giancola C and Pagano B 2013 Energetics of ligand binding to G-quadruplexes Top. Curr. Chem. 330 211–42
[42] Bončina M, Podlipnik Č, Piantanida I, Eilmes J, Teulade-Fichou M-P, Vesnaver G and Lah J 2015 Thermodynamic fingerprints of ligand binding to human telomeric G-quadruplexes Nucleic. Acids Res. 43 10376–86
[43] Musetti C, Krapcho A P, Palumbo M and Sissi C 2013 Effect of G-quadruplex polymorphism on the recognition of telomeric DNA by a metal complex PLoS One 8 e58529
[44] Clovis N S, Alam P, Chand A K, Sardana D, Khan M F and Sen S 2023 Molecular crowders modulate ligand binding affinity to G-quadruplex DNA by decelerating ligand association J. Photochem. Photobiol. A Chem. 437 114432
[45] Verma S D, Pal N, Singh M K, Shweta H, Khan M F and Sen S 2012 Understanding ligand interaction with different structures of G-quadruplex DNA: evidence of kinetically controlled ligand binding and binding-mode assisted quadruplex structure alteration Anal. Chem. 84 7218–26
[46] Clovis N S and Sen S 2022 G-Tetrad-selective ligand binding kinetics in G-quadruplex DNA probed with fluorescence correlation spectroscopy J. Phys. Chem. B 126 6007–15
[47] Paul S, Hossain S S, M Bala D and Samanta A 2019 Interactions between a bioflavonoid and c-MYC promoter G-quadruplex DNA: ensemble and single-molecule investigations J. Phys. Chem. B 123 2022–31
[48] Nakano S, Miyoshi D and Sugimoto N 2014 Effects of molecular crowding on the structures, interactions, and functions of nucleic acids Chem. Rev. 114 2733–58
[49] Zimmerman S B and Minton A P 1993 Macromolecular crowding: biochemical, biophysical, and physiological consequences Annu. Rev. Biophys. Biomol. Struct. 22 27–65
[50] Ellis R J 2001 Macromolecular crowding: an important but neglected aspect of the intracellular environment Curr. Opin. Struct. Biol. 11 114–9
[51] Arora A, Balasubramanian C, Kumar N, Agrawal S, Ojha R P and Maiti S 2008 Binding of berberine to human telomeric quadruplex – spectroscopic, calorimetric and molecular modeling studies FEBS J. 275 3971–83
[52] Chen Z, Zheng K, Hao Y and Tan Z 2009 Reduced or diminished stabilization of the telomere G-quadruplex and inhibition of telomerase by small chemical ligands under molecular crowding condition J. Am. Chem. Soc. 131 10430–8
[53] Heddi B and Phan A T 2011 Structure of human telomeric DNA in crowded solution J. Am. Chem. Soc. 133 9824–33
[54] Rastogi H and Chowdhury P K 2022 Correlating the local and global dynamics of an enzyme in the crowded milieu J. Phys. Chem. B 126 3208–23
[55] Rastogi H and Chowdhury P K 2021 Understanding enzyme behavior in a crowded scenario through modulation in activity, conformation and dynamics. Biochim. Biophys. Acta. Proteins. Proteom. 1869 140699
[56] Das N and Sen P 2022 Macromolecular crowding: how shape and interaction affect the structure, function, conformational dynamics and relative domain movement of a multi-domain protein Phys. Chem. Chem. Phys. 24 14242–56
[57] Das N and Sen P 2020 Shape-dependent macromolecular crowding on the thermodynamics and microsecond conformational dynamics of protein unfolding revealed at the single-molecule level J. Phys. Chem. B 124 5858–71
[58] Takahashi S and Sugimoto N 2020 Stability prediction of canonical and non-canonical structures of nucleic acids in various molecular environments and cells Chem. Soc. Rev. 49 8439–68
[59] Miller M C, Buscaglia R, Chaires J B, Lane A N and Trent J O 2010 Hydration is a major determinant of the G-quadruplex stability and conformation of the human telomere 3′ sequence of d(AG3(TTAG3)3) J. Am. Chem. Soc. 132 17105–7
[60] Köhn B, Schwarz P, Wittung-Stafshede P and Kovermann M 2021 Impact of crowded environments on binding between protein and single-stranded DNA Sci. Rep. 11 17682
[61] Dey P and Bhattacherjee A 2018 Role of macromolecular crowding on the intracellular diffusion of DNA binding proteins Sci. Rep. 8 844
[62] Zosel F, Soranno A, Buholzer K J, Nettels D and Schuler B 2020 Depletion interactions modulate the binding between disordered proteins in crowded environments Proc. Natl. Acad. Sci. 117 13480–9
[63] Yadav K, Sardana D, Shweta H, Clovis N S and Sen S 2022 Molecular picture of the effect of cosolvent crowding on ligand binding and dispersed solvation dynamics in G-quadruplex DNA J. Phys. Chem. B 126
[64] Gao C, Mohamed H I, Deng J, Umer M, Anwar N, Chen J, Wu Q, Wang Z and He Y 2023 Effects of molecular crowding on the structure, stability, and interaction with ligands of G-quadruplexes ACS Omega. 8 14342–8
[65] Ota C, Suzuki H, Tanaka S-I and Takano K 2022 Dispersion effect of molecular crowding on ligand-protein surface binding sites of escherichia coli RNase HI. Langmuir 38 14497–507
[66] Sarkar A, Gasic A G, Cheung M S and Morrison G 2022 Effects of protein crowders and charge on the folding of superoxide dismutase 1 variants: a computational study J. Phys. Chem. B 126 4458–71
[67] Patra S, Claude J-B, Naubron J-V and Wenger J 2021 Fast interaction dynamics of G-quadruplex and RGG-rich peptides unveiled in zero-mode waveguides Nucleic. Acids Res. 49 12348–57
[68] Speer S L, Zheng W, Jiang X, Chu I-T, Guseman A J, Liu M, Pielak G J and Li C 2021 The intracellular environment affects protein–protein interactions Proc. Natl. Acad. Sci. 118 e2019918118
[69] Speer S L, Stewart C J, Sapir L, Harries D and Pielak G J 2022 Macromolecular crowding is more than hard-core repulsions Annu. Rev. Biophys. 51 267–300

[70] Mukherjee S, Waegele M M, Chowdhury P, Guo L and Gai F 2009 Effect of macromolecular crowding on protein folding dynamics at the secondary structure level *J. Mol. Biol.* **393** 227–36
[71] Chung S, Lerner E, Jin Y, Kim S, Alhadid Y, Grimaud L W, Zhang I X, Knobler C M, Gelbart W M and Weiss S 2019 The effect of macromolecular crowding on single-round transcription by Escherichia coli RNA polymerase *Nucleic. Acids Res.* **47** 1440–50
[72] Kosiol N, Juranek S, Brossart P, Heine A and Paeschke K 2021 G-quadruplexes: a promising target for cancer therapy *Mol. Cancer* **20** 40
[73] Sarkar S, Bisoi A and Singh P C 2022 Spectroscopic and molecular dynamics aspect of antimalarial drug hydroxychloroquine binding with human telomeric G-quadruplex *J. Phys. Chem.* B **126** 5241–9
[74] Sarkar S, Bisoi A and Singh P C 2023 Antimalarial drugs induce the selective folding of human telomeric G-quadruplex in a cancer-mimicking microenvironment *J. Phys. Chem.* B **127** 6648–55
[75] Sardana D, Alam P, Yadav K, Clovis N S, Kumar P and Sen S 2023 Unusual similarity of DNA solvation dynamics in high-salinity crowding with divalent cations of varying concentrations *Phys. Chem. Chem. Phys.* **25** 27744–55
[76] Christiansen A, Wang Q, Samiotakis A, Cheung M S and Wittung-Stafshede P 2010 Factors defining effects of macromolecular crowding on protein stability: an in vitro/in silico case study using cytochrome c *Biochemistry* **49** 6519–30
[77] Ali A, Bidhuri P, Malik N A and Uzair S 2019 Density, viscosity, and refractive index of mono-, di-, and tri-saccharides in aqueous glycine solutions at different temperatures *Arabian J. Chem.* **12** 1684–94
[78] Hänsel R, Löhr F, Foldynová-Trantírková S, Bamberg E, Trantírek L and Dötsch V 2011 The parallel G-quadruplex structure of vertebrate telomeric repeat sequences is not the preferred folding topology under physiological conditions *Nucleic Acids Res.* **39** 5768–75
[79] Schasfoort R B M 2017 *Introduction to Surface Plasmon Resonance, Handbook of Surface Plasmon Resonance* (UK: The Royal Society of Chemistry)
[80] Porschke D 1998 Time-resolved analysis of macromolecular structures during reactions by stopped-flow electrooptics *Biophys. J.* **75** 528–37
[81] Li K, Yatsunyk L and Neidle S 2021 Water spines and networks in G-quadruplex structures *Nucleic Acids Res.* **49** 519–28
[82] Yaku H, Murashima T, Tateishi-Karimata H, Nakano S, Miyoshi D and Sugimoto N 2013 Study on effects of molecular crowding on G-quadruplex-ligand binding and ligand-mediated telomerase inhibition *Methods* **64** 19–27
[83] Prado E, Bonnat L, Bonnet H, Lavergne T, Van der Heyden A, Pratviel G, Dejeu J and Defrancq E 2018 Influence of the SPR experimental conditions on the G-quadruplex DNA recognition by porphyrin derivatives *Langmuir* **34** 13057–64
[84] Debnath M, Ghosh S, Panda D, Bessi I, Schwalbe H, Bhattacharyya K and Dash J 2016 Small molecule regulated dynamic structural changes of human G-quadruplexes *Chem. Sci.* **7** 3279–85
[85] Kawai K, Matsutani E, Maruyama A and Majima T 2011 Probing the charge-transfer dynamics in DNA at the single-molecule level *J. Am. Chem. Soc.* **133** 15568–77
[86] Choi J, Kim S, Tachikawa T, Fujitsuka M and Majima T 2011 pH-induced intramolecular folding dynamics of i-motif DNA *J. Am. Chem. Soc.* **133** 16146–53
[87] Yin Y, Yang L, Zheng G, Gu C, Yi C, He C, Gao Y Q and Zhao X S 2014 Dynamics of spontaneous flipping of a mismatched base in DNA duplex *Proc. Natl Acad. Sci.* **111** 8043–8
[88] Yadav R, Sengupta B and Sen P 2014 Conformational fluctuation dynamics of domain i of human serum albumin in the course of chemically and thermally induced unfolding using fluorescence correlation spectroscopy *J. Phys. Chem.* B **118** 5428–38
[89] Nandy A, Chakraborty S, Nandi S, Bhattacharyya K and Mukherjee S 2019 Structure, activity, and dynamics of human serum albumin in a crowded pluronic F127 hydrogel *J. Phys. Chem.* B **123** 3397–408
[90] Otosu T, Ishii K and Tahara T 2015 Microsecond protein dynamics observed at the single-molecule level *Nat. Commun.* **6** 7685
[91] Sasmal D K, Mondal T, Sen Mojumdar S, Choudhury A, Banerjee R and Bhattacharyya K 2011 An FCS study of unfolding and refolding of CPM-labeled human serum albumin: role of ionic liquid *J. Phys. Chem.* B **115** 13075–83
[92] Kistwal T, Mukhopadhyay A, Dasgupta S, Sharma K P and Datta A 2022 Ultraslow biological water-like dynamics in waterless liquid protein *J. Phys. Chem. Lett.* **13** 4389–93
[93] Pratyusha V A *et al* 2018 Ras hyperactivation versus overexpression: lessons from Ras dynamics in Candida albicans *Sci. Rep.* **8** 5248
[94] Garai K, Sureka R and Maiti S 2007 Detecting amyloid-β aggregation with fiber-based fluorescence correlation spectroscopy *Biophys. J.* **92** L55–7
[95] Wennmalm S, Chmyrov V, Widengren J and Tjernberg L 2015 Highly sensitive FRET-FCS detects amyloid β-peptide oligomers in solution at physiological concentrations *Anal. Chem.* **87** 11700–5
[96] Al-Soufi W, Reija B, Novo M, Felekyan S, Kühnemuth R and Seidel C A M 2005 Fluorescence correlation spectroscopy, a tool to investigate supramolecular dynamics: inclusion complexes of pyronines with cyclodextrin *J. Am. Chem. Soc.* **127** 8775–84
[97] Pal N, Verma S D, Singh M K and Sen S 2011 Fluorescence correlation spectroscopy: an efficient tool for measuring size, size-distribution and polydispersity of microemulsion droplets in solution *Anal. Chem.* **83** 7736–44
[98] Khan M F, Singh M K and Sen S 2016 Measuring size, size distribution, and polydispersity of water-in-oil microemulsion droplets using fluorescence correlation spectroscopy: comparison to dynamic light scattering *J. Phys. Chem.* B **120** 1008–20
[99] Sharma S, Pal N, Chowdhury P K, Sen S and Ganguli A K 2012 Understanding growth kinetics of nanorods in microemulsion: a combined fluorescence correlation spectroscopy, dynamic light scattering, and electron microscopy study *J. Am. Chem. Soc.* **134** 19677–84
[100] Caldin E F 2001 *The Mechanisms of Fast Reactions in Solution* (IOS Press)
[101] Le H T, Dean W L, Buscaglia R, Chaires J B and Trent J O 2014 An investigation of G-quadruplex structural polymorphism in the human telomere using a combined approach of hydrodynamic bead modeling and molecular dynamics simulation *J. Phys. Chem.* B **118** 5390–405